A Novel Approach Utilizing Graphene-Based Microfluidic Technology for Skin Cancer Detection

Marwa Rezeg*, Aymen Hlali, Afef Oueslati, and Hassen Zairi

Research Laboratory Smart Electricity & ICT, SEICT, National Engineering School of Carthage
University of Carthage, Tunis, Tunisia

ABSTRACT: The introduction of microfluidics technology with graphene provides many advantages, such as improving the selectivity and sensitivity, achieving chemical and thermal stability, decreasing the size of devices, and improving the cell and biological response of the substance. The principal objective of this paper is to compare the constitutive parameters in order to develop graphene-based microfluidic sensors. The simulation results illustrate that the suggested sensor exhibits a strong ability to detect normal skin tissue with an excellent sensitivity of 6.060 (THz/RIU) and to identify skin cancer with a notably significant sensitivity of 4.59 THz/RIU. Additionally, it shows considerable figure of merits, with values of 550.9 and 353.61 RIU, respectively. In conclusion, the simplicity, effectiveness, and adjustability of the proposed biosensor render it well suited for skin tumor detection.

1. INTRODUCTION

The terahertz (THz) radiation is generally defined as the area of the electromagnetic spectrum from 100 GHz to 10 THz [1]. The scientific community has shown significant interest in the utilization of terahertz waves as excitation waves for sensing and imaging applications, thanks to the advancements in terahertz technology.

In recent years, the field of terahertz (THz) technology has garnered interest from biological research laboratories because of its noninvasive, contactless, and nondestructive method for optically detecting biological substances without the need for labeling [2, 3]. In addition, THz waves are an important tool for biosensor applications due to their low energy, which makes them suitable for sensing and detecting chemical, pharmaceutical, and biological molecules. Due to their low energy, THz waves can penetrate a wide variety of materials without causing damage.

The rapid development of biosensing platforms over the last few years has caused a revolutionary impact in the fields of physics [4] and biomedicine [5], it is being explored for its potential in DNA detection [6], melanoma diagnostics [7], SARS-CoV-2 detection [8], glucose Detection [9], and virus sensing [10]. Furthermore, biosensors have emerged as a promising tool for cancer detection, offering fast and accurate results. It can be based on various structures and technologies, each with its unique advantages and applications including; coplanar waveguide structure [11], interdigitated electrodes [12], ring resonator [13], and metamaterial structure [14]. The choice of biosensor structure depends on the specific application, target analyte, and the desired level of sensitivity and specificity.

Recent research has focused on the development of biosensors by incorporating novel materials such as graphene sheets. Graphene sheets have been found to be important in terms of

sensor performance due to their unique physical, chemical, and electrical properties. Graphene is a zero-bandgap semiconductor, and its bandgap can be tuned by surface modification, making it an ideal material for the construction of field-effect transistor (FET) biosensors [15]. The p-orbital electrons of graphene form π bonds with the surrounding atoms, and the electrons of these π bonds have high sensitivity to any environmental change, making graphene materials very suitable for chemical and biosensor applications [16]. The large surface area of graphene and its high electrical conductivity make it an ideal candidate for the development of highly sensitive and selective biosensors [17]. Several studies have explored the use of graphene-based biosensors for cancer detection, such as breast cancer [18], basal cancer [19], and blood cancer [20]. The studies highlighted the potential of graphene for cancer detection.

Since the development of graphene-based microfluidic biosensors, there has been a significant advancement in the field of biomedical diagnostics, offering unprecedented sensitivity and rapid detection capabilities for various biomolecules and pathogens. Compared with traditional sensing systems, the integration of graphene with microfluidics offers numerous benefits, including enabling miniaturization, reducing response times and chemical consumption, and enhancing device reproducibility and sensitivity.

The rapid progress of Microfluidics Technology has attracted broad interest across various fields. A microfluidic biosensor serves as an analytical platform that facilitates the specific diagnosis of localized tumor cells and circulating tumor cells by converting biological signals into quantifiable data [21].

Graphene is considered a very optimal material for designing microfluidic devices due to its widespread recognition in both fundamental and practical research areas, thanks to its remarkable electrical, mechanical, and chemical properties [22]. In the diagnosis of tumor cells, graphene-based biosensors have pre-

---

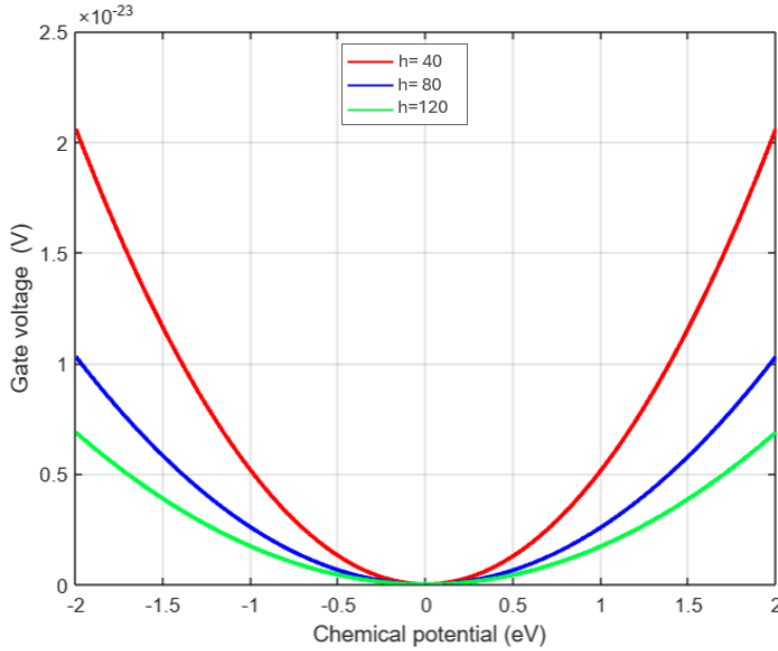* Corresponding author: Marwa Rezeg (marwa.rezeg@enicar.ucar.tn).

FIGURE 1. The gate voltage as a function of chemical potential.

sented significant performance with excellent properties such as conductivity, biocompatibility, sensitivity, selectivity, stability, and a wide detection range [23].

Graphene excels in heat transfer compared to other materials, displaying high electron transfer rates, excellent charge-carrier mobility, reduced electrical noise levels, and low planar density ($0.77\,\text{mg/m}^2$) [24, 25]. In addition, the incorporation of graphene enhances the biocompatibility of the microfluidic device with certain biomolecules, including cells [26].

The aim of this article is to present a graphene-based biosensor that can be adjusted for noninvasive, label-free detection, specifically designed to operate within the terahertz frequency range. The design is based on a circular capacitor structure using an integrated device technology on a quartz substrate. This paper is organized as follows. Section 2 is dedicated to biosensor design description and analytical model. Section 3 deals with the experimental validation of the approach and a discussion of the results that have been obtained.

2. THEORY AND FORMULATION

2.1. Graphene Complex Conductivity

Graphene has garnered significant research interest among scientists thanks to remarkable advancements in fundamental research and promising real-world applications [27, 28]. Graphene is recognized by its outstanding surface conductivity and can be described particularly by considering the intraband contribution, which can be assessed by

$$\sigma_{\text{intra}} = -j\frac{e^2 k_B T}{\pi \overline{h}^2 (\omega - j2\Gamma)}\left[\frac{\mu_c}{K_B T} + 2\ln\left(e^{\left(-\frac{\mu_c}{K_B T}\right)} + 1\right)\right] \quad (1)$$

where e is the electron charge, K_B the Boltzmann constant, ω the angular frequency, $\overline{h}$ the reduced Plank constant, Γ is the phenomenological scattering rate, μ_c the chemical potential, and T the temperature in Kelvin.

2.2. Gate Voltage

The modification of gate voltage has the capability to fine-tune the conductivity of graphene [29]. The correlation between chemical potential μ_c and gate voltage V_g is expressed as follows:

$$V_g = \frac{e\mu_c^2 h}{\pi h^2 V_f^2 \epsilon_0 \epsilon_r} \quad (2)$$

where h represents the substrates thickness, ϵ_r the relative electric permittivity of the substrate, ϵ_0 the electric permittivity of free space, and V_f the fermi velocity of graphene. Fig. 1 represents the gate voltage as a function of chemical potential for different values of substrate thickness.

2.3. Proposed Biosensor Design

The proposed biosensor is designed for sample sensing using a circular finger-type interdigital capacitor. Circular interdigital electrodes are employed to achieve a localized electric field concentration. Graphene is selected as the material for the electrodes because this noble metal is biocompatible and has the ability to directly interact with biological substances. For this purpose, a coplanar waveguide transmission line is used.

A schematic drawing of the biosensors is shown in Fig. 2. To investigate cells within a liquid environment, we introduce a microfluidic channel made of polydimethylsiloxane (PDMS) with permittivity $\epsilon_r = 1.8$ and loss tangent values $\tan\delta = 0.035$, on the upper surface of a quartz substrate.
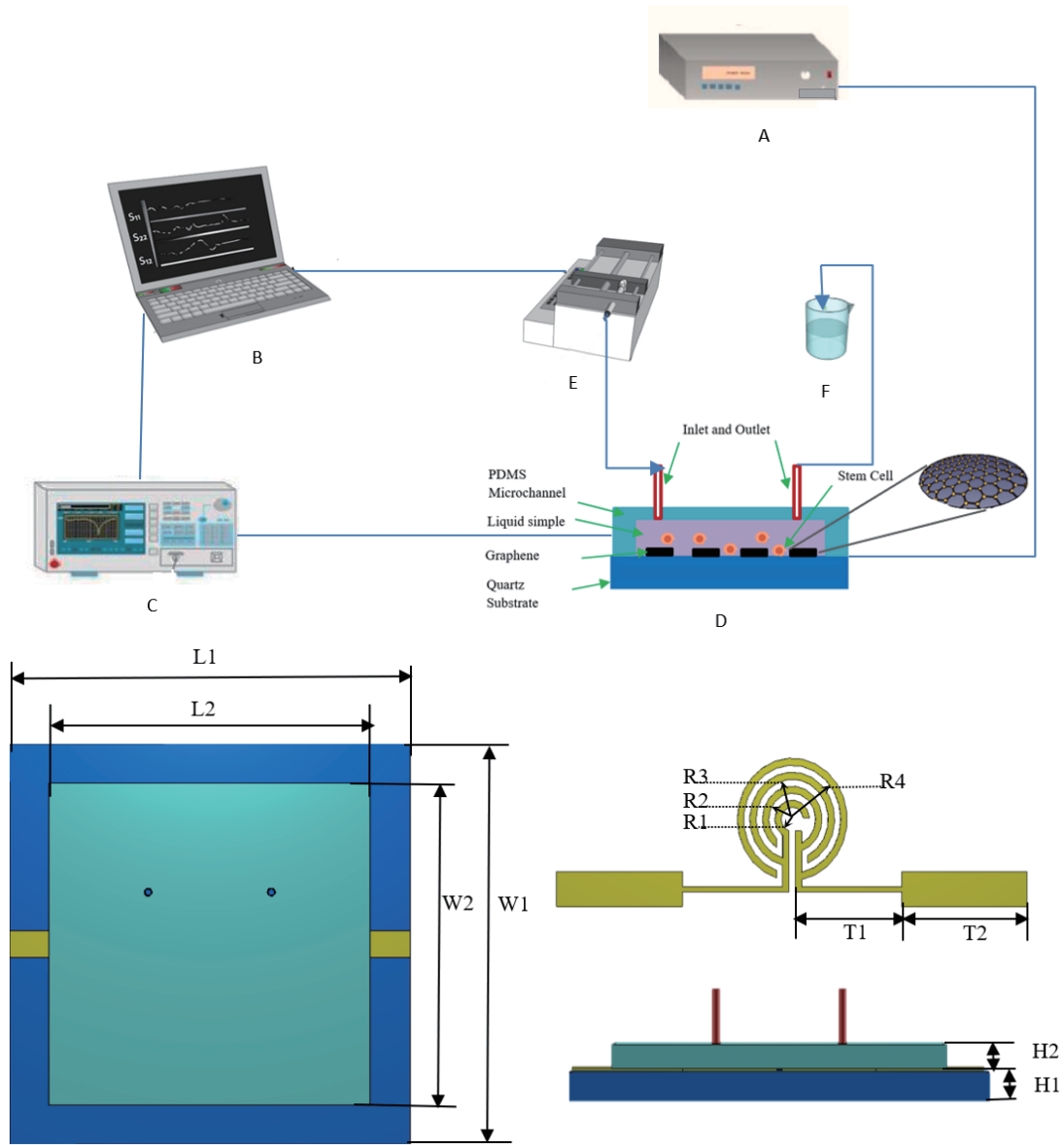
FIGURE 2. Schematic representation of the proposed biosensor. The setup consists of a THz generator, a computer, an optical spectrum analyzer, a microfluidic biosensor, a syringe pump, and a waste container as indicated in A through F, respectively.

The values of the biosensor dimensions are provided in Table 1.

Interdigital capacitors (IDCs) are applied in biological sensors, where the interaction between the analyte and a sensitive layer induces alterations in capacitance or impedance. The overall capacitance of the IDC is determined by several factors and can be represented as:

$$C_{\text{total}} = (N - 3)\left(\frac{C_1}{2}\right) + 2\left(\frac{C_1 C_E}{C_1 + C_E}\right), \text{ for } N > 3 \quad (3)$$

where N is the total number of interdigital fingers, C_1 the capacitance of an interior unit cell, and C_E the capacitance of an exterior unit cell. The two capacitances are determined by:

$$C_1 = \epsilon_0 L\left(\frac{K(k_{\text{I}\infty})}{K(k'_{\text{I}\infty})} + (\epsilon_1 - 1)\frac{K(k_{\text{I}1})}{K(k'_{\text{I}1})} + \epsilon_s\frac{K(k_{\text{I}\infty})}{K(k'_{\text{I}\infty})}\right) \quad (4)$$

$$C_E = \epsilon_0 L\left(\frac{K(k_{\text{E}\infty})}{K(k'_{\text{E}\infty})} + (\epsilon_1 - 1)\frac{K(k_{\text{E}1})}{K(k'_{\text{E}1})} + \epsilon_s\frac{K(k_{\text{E}\infty})}{K(k'_{\text{E}\infty})}\right) \quad (5)$$

where L is the circular finger length, and $K(k)$ is the complete elliptic integral of first kind with modulus k and complementary modulus with:

$$k' = \sqrt{1 - k^2} \quad (6)$$

$$k_{\text{I}\infty} = \frac{\sin \pi\eta}{2} \quad (7)$$

$$k_{\text{E}\infty} = \frac{2\sqrt{\eta}}{1 + \eta} \quad (8)$$

The resonance frequency f_r of the biosensor under consideration is influenced by inductance L and capacitance C of the

TABLE 1. The optimal dimensions of the proposed biosensor.

Parameter	Value (μm)	Parameter	Value (μm)
L_1	1500	R_1	35
L_2	1200	R_2	75
W_1	1500	R_3	115
W_2	1200	R_4	155
L_g	20	T_1	340
H_1	40	T_2	400
H_2	50	-	-

structure. This relationship can be articulated as follows:

$$f_r = \frac{1}{2\pi\sqrt{LC_0}} \qquad (9)$$

and

$$C_0 = C_{\text{total}} + C_{\text{var}} \qquad (10)$$

with C_{var} being the varactor capacitance value.

3. RESULTS AND DISCUSSION

The microfluidic biosensor is simulated using CST Studio. In the initial phase, gold material is employed to create the top structure instead of copper in order to achieve the adjustment of the bandwidth and resonance frequency. Graphene is added in the sensitive area of detection in the next step, according to Fig. 3. The results of simulations using various materials are depicted in Fig. 4, with the graphene characteristics set as follows: $\mu_c = 0.1\,\text{eV}$, $\tau = 0.1\,\text{ps}$, and $T = 300\,\text{K}$. The final result shows that the reflection coefficient S_{22} is $-51.41\,\text{dB}$ at $0.94\,\text{THz}$. It is evident from this figure that the inclusion of the graphene layer enhances the result. In the presence of copper and gold, the reflection coefficient of the biosensor is not adapted, and the peak is not well optimized. Modifying the graphene parameters can effectively tune the surface conductivity without the need to alter the physical properties of the component. This will be further explored in the following investigation.

The modification of graphene's chemical potential μ_c leads to changes in both the bandwidth and resonance frequency of our graphene-based biosensor. Figs. 5 and 6 illustrate how the suggested biosensor can be adjusted as the chemical potential ranges from $0.1\,\text{eV}$ to $0.5\,\text{eV}$. The analysis of Fig. 5 shows the chemical potential variation versus reflection coefficient and resonance frequency, and the reflection coefficient corresponds to $-51.41\,\text{dB}$ at $0.94\,\text{THz}$ when the chemical potential matches $0.1\,\text{eV}$; however, the amplitude of the reflection coefficient decreases and attains $-31.71\,\text{dB}$ at $0.947\,\text{THz}$ when the chemical potential equals $0.5\,\text{eV}$. It can be concluded from changing chemical potential between higher and lower frequencies that this parameter is varied for each structure. Furthermore, it is evident that the amplitude of the resonance frequency depth is enhanced as the chemical potential varies. Fig. 6 shows that as the relaxation time increases from 0.1 to $0.5\,\text{ps}$, there is a slight shift in both the resonance frequency and the bandwidth.

One of the most interesting characteristics of graphene is its relaxation time, which is a crucial parameter in determining the material's properties and behavior. Figs. 7 and 8 depict the impact of the relaxation time on the bandwidth and resonance frequency of the proposed biosensor under unloaded conditions.

From Fig. 7 we can note that, as the relaxation time τ of graphene varies from $0.1\,\text{ps}$ to $0.6\,\text{ps}$, the resonance frequency's position shifts, and the reflection coefficient corresponds to $-51.41\,\text{dB}$ at $0.94\,\text{THz}$ when the relaxation time matches $0.1\,\text{ps}$. However, the amplitude of the reflection coefficient decreases and attains $-37.5\,\text{dB}$ at $0.942\,\text{THz}$ when the relaxation time equals $0.6\,\text{ps}$. The variation of resonance frequency and bandwidth versus relaxation time are depicted in Fig. 8. When increasing the values of relaxation time the resonance frequency shifted to higher frequencies, and the bandwidth decreased. It appears that adjusting the relaxation time to $0.1\,\text{ps}$ can optimize the performance of the presented biosensor. Therefore, the selection of $0.1\,\text{ps}$ as the relaxation time is based on its potential to enhance the sensitivity and overall performance of the biosensor, making it a critical parameter in biosensor optimization.

On the other hand, the variation in the temperature is shown in Figs. 9 and 10. It is clear that the temperature T is variable in Equation (1). Therefore, this parameter affects the conductivity, then affects the performance of the biosensor. With the variation of temperature from $100\,\text{K}$ to $800\,\text{K}$, it is evident from Fig. 10 that the most suitable temperature is $600\,\text{K}$, leading to an improvement in the reflection coefficient. In Fig. 9, the reflection coefficient corresponds to $-64.25\,\text{dB}$ at $0.94\,\text{THz}$ when the temperature conforms to $600\,\text{K}$.

The suggested biosensor exhibits a wide bandwidth and notably higher sensitivity than the one described in [30].

Subsequently, the effectiveness of the proposed microfluidic biosensing platform is evaluated for its capability to detect changes in the refractive index of the surrounding medium. In order to justify the capability of the proposed biosensor for cell investigation, different simulations were performed using agar-based culture support, healthy skin, and pigmentary skin.

4. HEALTHY SKIN TISSUE AND PIGMENTARY SKIN CANCER DETECTION AND SENSING

To explore the sensing characteristics of the suggested biosensor, the detection area within the interdigitated circular capacitor is filled with the test samples using channels designed to hold aqueous solutions. To enhance the device's reliability and prevent any potential fluid seepage, inlet and outlet connectors
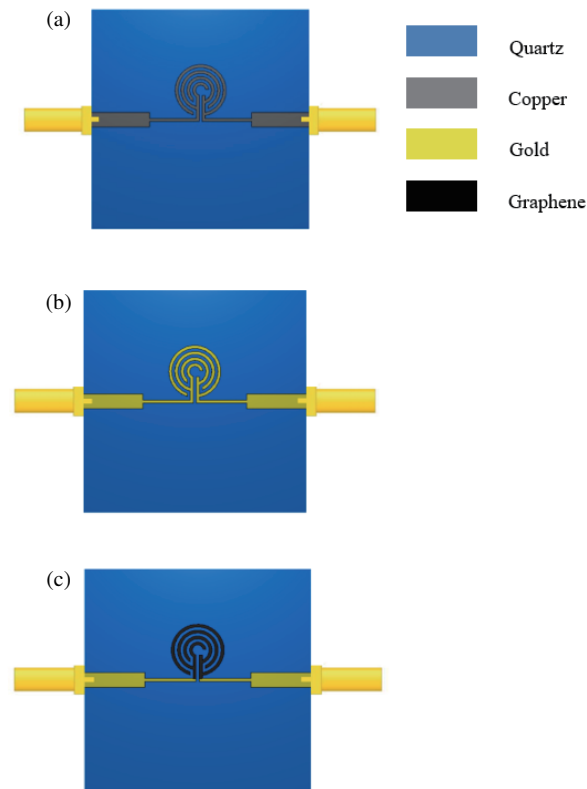
FIGURE 3. Sensor design process, (a) copper-based biosensor, (b) gold-based biosensor, (c) graphene-based biosensor for $N = 4$.
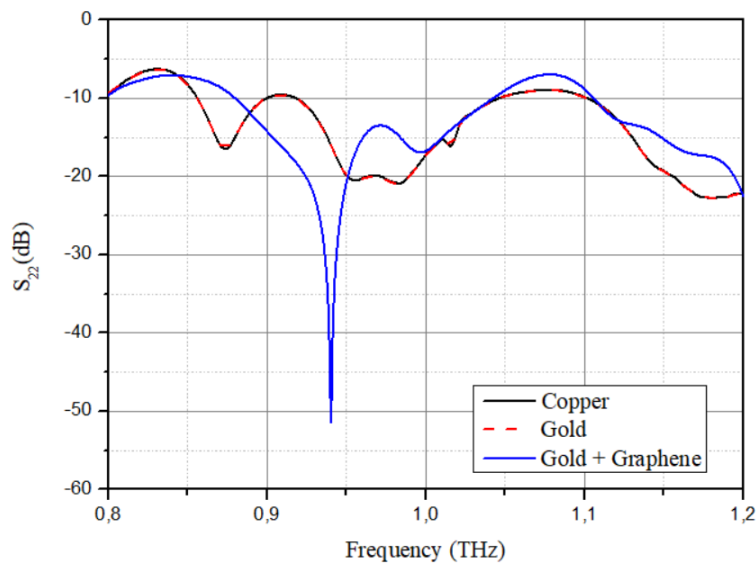

FIGURE 4. Diverse material simulations of a graphene-based biosensor.

were affixed to the PDMS cover. First of all, in order to justify the capability of biosensor for liquid investigation, simulations were performed using agar-based culture support.

The agar liquid is a highly effective medium for nurturing and cultivating cells. It provides an abundant supply of essential nutrients and oxygen to support the growth of microorganisms. This oxygen-enriched solution is widely utilized in laboratories [31]. Fig. 11 illustrates our approach frequency response where the sensing area is covered with a low volume of agar. The parameters are fixed to $\tau = 0.1$ and $T = 300\,\mathrm{K}$ and $\mu_c = 0.1$. As observed, when our biosensor was loaded with an agar sample, a significant shift in the reflection coefficient occurred, with the peak reaching -45.44 at 0.93 THz.
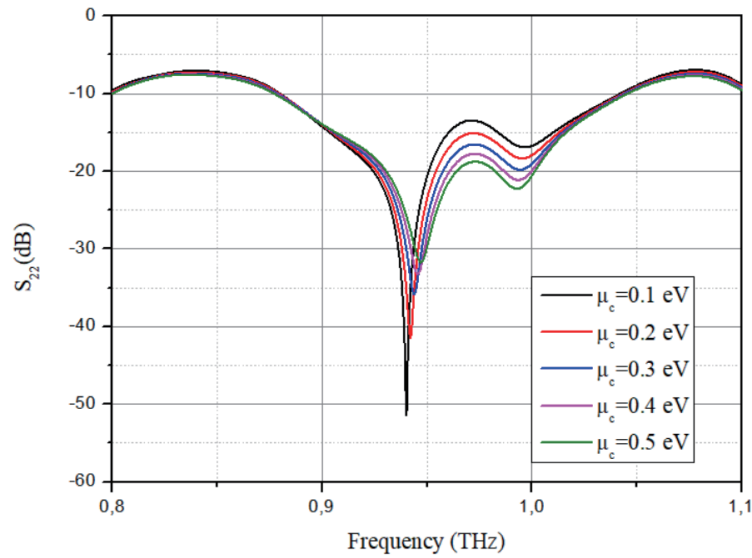
FIGURE 5. Analyzing simulation results: impact of chemical potential variation in graphene-based sensor.
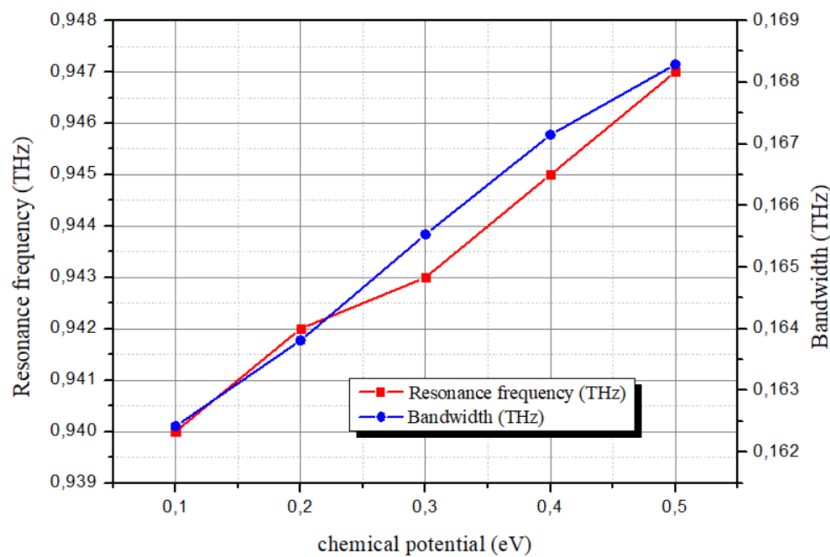

FIGURE 6. Analyzing the influence of chemical potential (0.1–0.5 eV) on the variability of resonance frequency and bandwidth.

The significant difference in the complex permittivities of samples within the terahertz spectral range offers the potential for early and noninvasive detection of the most dangerous skin cancer (Pigmentary Skin) precursors of melanoma. EM simulations have been validated with an 8 μm diameter of bio-objects under test. These spheres represent a dielectric cell model located between interdigitated electrodes. The permittivity and conductivity of healthy skin are respectively 2.76 and 0.001 S/m extracted from previous literature [32, 33]; moreover, the permittivity and conductivity of skin cancer are 3.5 and 0.02 S/m [34, 35]. The resonance frequency shift is shown in Fig. 12. As evident, the suggested biosensor exhibits a notable shift in the reflection coefficient towards higher frequencies.

Regarding biosensors, the essential metrics for evaluating sensing performance include sensitivity (S), figure of merit (FOM), and quality factor. These parameters are defined in [36] and [37].

$$\text{Sensitivity} = \frac{\Delta f}{\Delta n}(THz/RUI) \qquad (11)$$

$$\text{Figure of Merits} = \frac{\text{Sensitivity}}{\text{Full-Width at Half-Maximum}}(RUI^{-1}) \quad (12)$$

$$\text{Quality-factor} = \frac{f_{res}}{\text{Full-Width at Half-Maximum}} \qquad (13)$$

where Δf and Δn represent:
- The changes in resonance frequency ($\Delta f = f_{Air} - f_{(\text{Healthy skin or Cancer skin})}$)
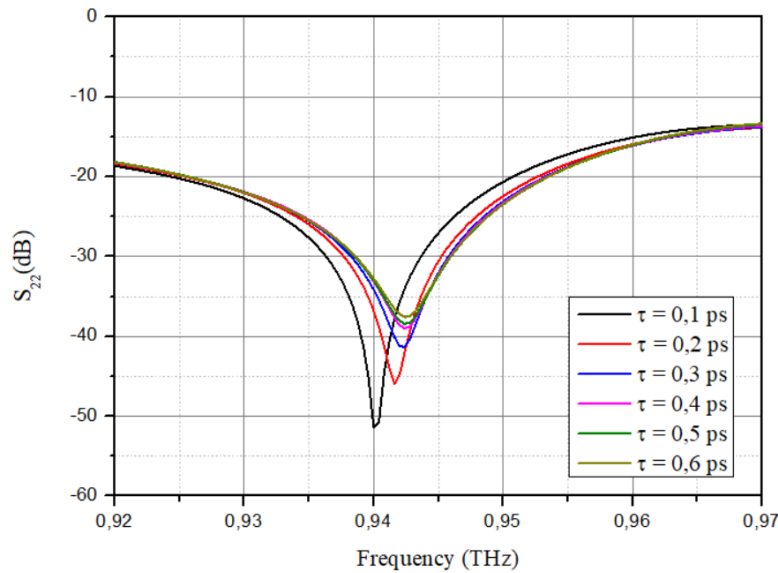
94

FIGURE 7. Analyzing simulation results: impact of relaxation time variation in graphene-based sensor.
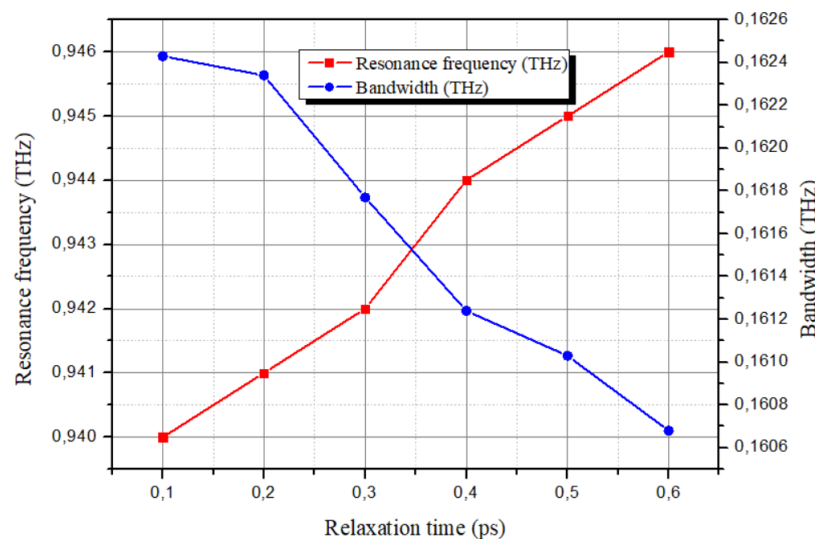

FIGURE 8. Analyzing the influence of relaxation time Values (0.1 to 0.6 p) on the variability of resonance frequency and bandwidth.

- The refractive index $\left(\Delta n = n_{Air} - n_{(\text{Healthy skin or Cancer skin})}\right)$

Compared to that of air ($n = 1$), referring to sources [38] and [39], the refractive indices of air, healthy, and cancer skin tissues are designated as $n_A = 1$, $n_H = 1.66$, and $n_C = 1.87$, respectively.

The THz biosensor, introduced in our study, is evaluated with different types of both normal and cancerous skin cells, considering their refractive index characteristics. The results are detailed in Table 2. From the table, a maximum sensitivity of 6.060 THz/RIU is inferred for detecting healthy skin, and the lowest sensitivity of 4.597 THz/RIU is noted for cancer tissue. This highlights the biosensor's precision in accurately detecting variations in refractive index.

The biosensor exhibits remarkable capability in discerning variations in refractive indices, as demonstrated by its figure of merit (FOM) values, which span from 353.61 to 550.90 RUI^{-1} for normal and cancerous skins. The figure of merit is an important parameter used to evaluate the performance of the biosensor. It is a measure of the overall effectiveness of the biosensor and is calculated based on sensitivity. Therefore, the FOM value of 550.90 RUI^{-1} reflects the strong potential of the graphene-based biosensor for accurate and reliable cancer cell detection. However, it is important to note that the figure of merit is not the only parameter that should be considered when biosensors are evaluated. Other important parameters include quality factor. Quality factor is a critical parameter that characterizes the accuracy of the transmittance reduction. The Q
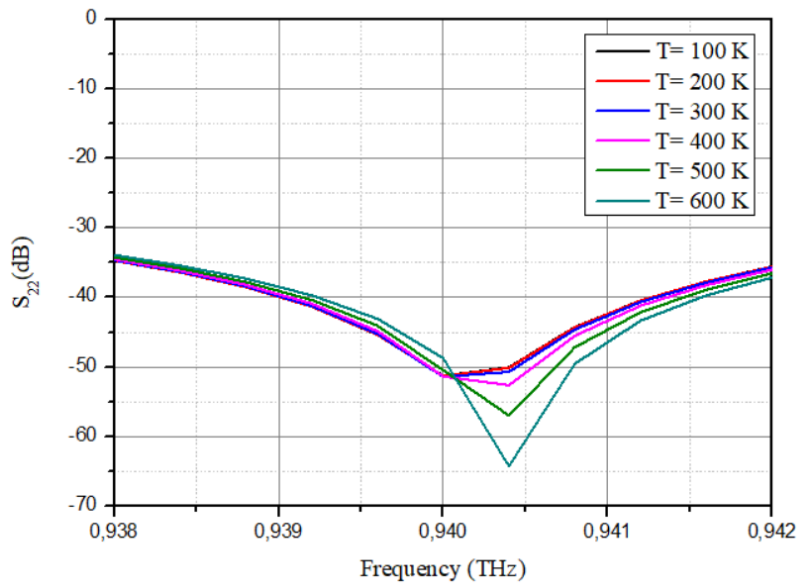
FIGURE 9. Analyzing simulation results: impact of temperature variation in graphene-based sensor (under unloaded case).
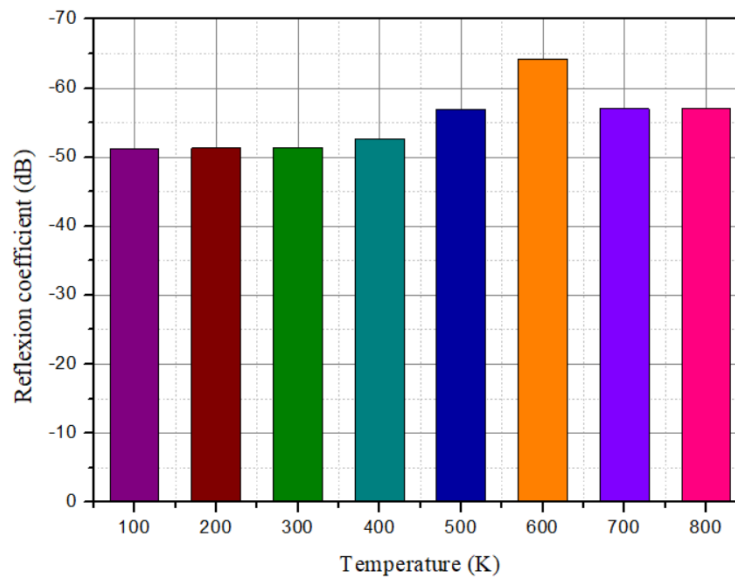

FIGURE 10. Variation of reflection coefficient vs different values of temperature from 100 K to 800 K at 0.94 THz.

values span from 72.33 to 85.49, highlighting its exceptional precision in detecting even the slightest changes in transmittance. Under the unloaded case, the quality factor is 78.33 at 0.94 THz, and excellent results were obtained with the highest value of 85.49 by loading the detection area with healthy skin tissue.

The proposed biosensor demonstrates remarkable precision, as indicated by the smallest Full-Width at Half-Maximum (FWHM) value, which measures just 0.012 THz. In summary, these parameters suggest strong performance, affirming that the designed structure is highly effective and suitable for cost-effective, timely, and efficient skin cancer detection. One of the notable characteristics of graphene is its adjustable con-

ductivity, influenced by variations in chemical potential and manageable through bias voltage control. The impact of altering graphene's chemical potential on sensitivity is detailed in Tables 3 and 4. The variation of chemical potential between 0.1 eV and 0.5 eV in the biosensor loaded with normal cells is presented in Table 3. As shown, this variation leads to a higher sensitivity of 6.060 at 0.9404 THz with a return loss about -54.363 dB when the chemical potential value is 0.1 eV. Table 4 shows that in cancer skin tissue, a higher sensitivity is achieved when μ_c equals 0.1 eV, leading to an enhancement in the reflection coefficient level.

Conversely, the characteristics of graphene's surface plasmons are highly influenced by the neighboring dielectric

TABLE 2. Characteristics of the biosensor for air, healthy and cancer skin tissue.

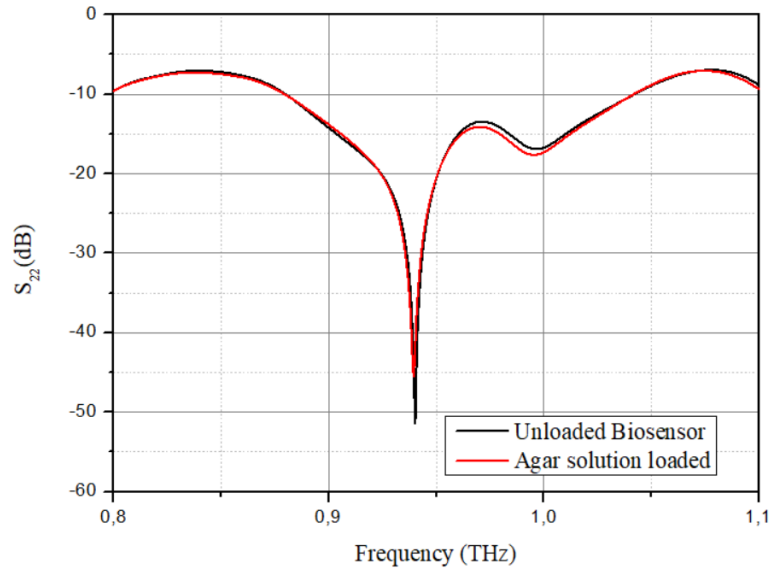| Refractive index	Resonance frequency (THz)	Return loss (dB)	Sensitivity (THz/RUI)	FWHM (THz)	FOM (RUI^{-1})	Q factor
Air ($n = 1$)	0.9400	-51.410	-	0.012	-	78.33
Healthy ($n = 1.66$)	0.9404	-54.363	6.060	0.011	550.90	85.49
Cancer ($n = 1,87$)	0.9404	-50.960	4.597	0.013	353.61	72.33

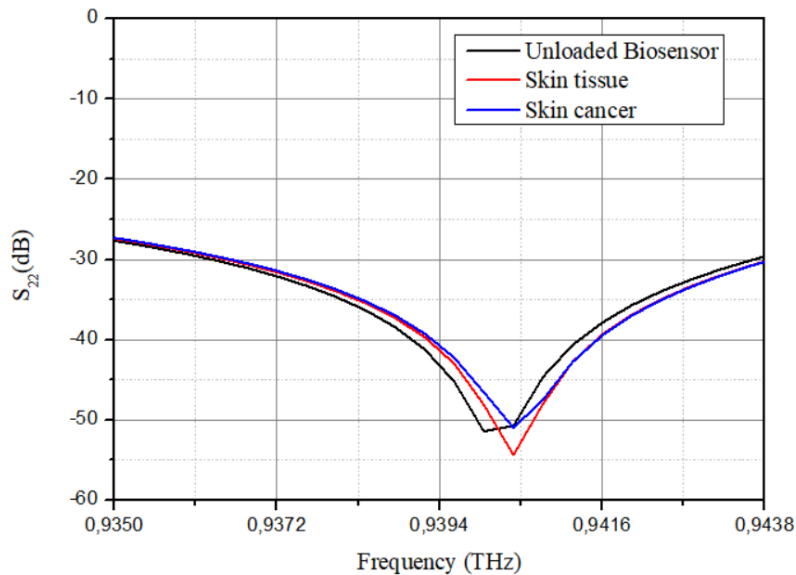**FIGURE 11**. Simulation results of the graphene-based biosensor loaded with Agar medium.

FIGURE 12. Simulation results of the graphene-based biosensor loaded with different skin cells.

medium. Therefore, any alteration in the dielectric's refractive index leads to modifications in graphene's surface plasmon properties and resonance frequency. It is important to highlight that the chemical potential depends on carrier density, and, as a result, the interaction between carriers' chemical potential and biological samples can significantly impact detection parameters.

We have compared the sensing parameters of the graphene-based structure with those from other studies, as detailed in Table 5. The table reveals that compared to most of the prior re-

TABLE 3. Comparison of the sensitivity with different values of chemical potential for healthy skin.

Potential (eV)	Resonance frequency (THz)	Return loss (dB)	Sensitivity (THz/RUI)
0.1	**0.9404**	**−54.363**	**6.060**
0.2	0.9424	−41.197	0.003
0.3	0.9444	−35.861	0.006
0.4	0.9464	−33.179	0.009
0.5	0.9474	−31.804	0.011

TABLE 4. Comparison of the sensitivity with different values of chemical potential for cancer skin.

Potential (eV)	Resonance frequency (THz)	Return loss (dB)	Sensitivity (THz/RUI)
0.1	**0.9404**	**−54.963**	**4.59**
0.2	0.9424	−41.912	0.002
0.3	0.9442	−36.105	0.004
0.4	0.9461	−33.405	0.006
0.5	0.9476	−31.881	0.008

TABLE 5. Examining our biosensor: A comparative analysis of sensing parameters in relation to other studies.

Reference	Sensitivity (THz/RUI)	FOM (RUI^{-1})	f_{Res} (THz)
[40]	0.13	1.04	3.7
[41]	1.96	19.86	3
[42]	1.6	8.27	1.15
[43]	1.90	6.56	9.046
This work	**6.060**	**550,90**	**0.94**

search, our proposed sensor exhibits favorable attributes, particularly in terms of sensitivity and figure of merit. These attributes position this biosensor as a promising candidate for future medical sensing applications. It is apparent that in majority of the prior studies, sensors typically possess only one favorable characteristic, either sensitivity or figure of merit, but not both simultaneously.

For instance, in [40], the sensitivity is modest, yet the figure of merit is relatively high. Furthermore, [41] stands out with a significantly high figure of merit, peaking at 19.8 RUI^{-1}; however, the sensitivity remains comparatively low at 1.96 THz/RIU. Nonetheless, the sensor presented in this paper exhibits strong detection capabilities on multiple fronts. It attains an impressive sensitivity of 6.060 THz/RIU and boasts a substantial figure of merit value, reaching 550.90 RIU^{-1} for skin tissue detection.

5. CONCLUSION

In this study, a microfluidic terahertz biosensor is designed with the aim of early skin cancer diagnosis to facilitate more efficient treatments for pigmentary skin nevi. An improvement is observed when graphene is used instead of copper and gold, thanks to graphene's high conductivity and sensitivity. Accordingly, the introduction of microfluidics technology with graphene provides many advantages, such as improving the se-

lectivity and sensitivity, achieving chemical and thermal stability, decreasing the size of devices, and improving the cell and biological reactivity of the material. The proposed sensor demonstrates effective detection of normal skin tissue with a sensitivity of 6.060 (THz/RIU) and skin cancer with a sensitivity of 4.59 THz/RIU, along with a figure of merit of 550.90 and 353.61 RIU^{-1}, respectively. The significant figure of merit and sensitivity for our proposed biosensor are crucial indicators of its performance. In summary, the high sensitivity of our terahertz-based sensor makes it highly suitable for a range of healthcare applications.

REFERENCES

[1] Han, K., T. K. Nguyen, I. Park, and H. Han, "Terahertz Yagi-Uda antenna for high input resistance," *Journal of Infrared, Millimeter, and Terahertz Waves*, Vol. 31, 441–454, 2010.

[2] Aloui, R., H. Zairi, F. Mira, I. Llamas-Garro, and S. Mhatli, "Terahertz antenna based on graphene material for breast tumor detection," *Sensing and Bio-Sensing Research*, Vol. 38, 100511, 2022.

[3] Mallik, S., P. K. Singh, G. Ahmad, S. Guhathakurata, S. S. Mahato, and N. B. Manik, "High-sensitive terahertz biosensors," *Advanced Materials for Future Terahertz Devices, Circuits and Systems*, Vol. 727, 289–314, 2021.

[4] Puigmartí-Luis, J., "Microfluidic platforms: A mainstream technology for the preparation of crystals," *Chemical Society Re-*

views, Vol. 43, No. 7, 2253–2271, 2014.

[5] Ma, J., S. M.-Y. Lee, C. Yi, and C.-W. Li, "Controllable synthesis of functional nanoparticles by microfluidic platforms for biomedical applications — A review," *Lab on A Chip*, Vol. 17, No. 2, 209–226, 2017.

[6] Weisenstein, C., D. Schaar, A. K. Wigger, H. Schäfer-Eberwein, A. K. Bosserhoff, and P. H. Bolívar, "Ultrasensitive THz biosensor for PCR-free cDNA detection based on frequency selective surfaces," *Biomedical Optics Express*, Vol. 11, No. 1, 448–460, 2020.

[7] Richter, M., Y. Loth, A. K. Wigger, D. Nordhoff, N. Rachinger, C. Weisenstein, A. K. Bosserhoff, and P. H. Bolívar, "High specificity thz metamaterial-based biosensor for label-free transcription factor detection in melanoma diagnostics," *Scientific Reports*, Vol. 13, 2023.

[8] Ahmadivand, A., B. Gerislioglu, Z. Ramezani, A. Kaushik, P. Manickam, and S. A. Ghoreishi, "Functionalized terahertz plasmonic metasensors: Femtomolar-level detection of SARS-CoV-2 spike proteins," *Biosensors and Bioelectronics*, Vol. 177, 112971, Apr. 2021.

[9] Oueslati, A., A. Hlali, and H. Zairi, "Numerical investigation of a new sensor for blood glucose detection using an improved wave concept iterative process method," *International Journal of Numerical Modelling — Electronic Networks, Devices and Fields*, Vol. 35, No. 5, e3001, 2022.

[10] Amin, M., O. Siddiqui, H. Abutarboush, M. Farhat, and R. Ramzan, "A THz graphene metasurface for polarization selective virus sensing," *Carbon*, Vol. 176, 580–591, May 2021.

[11] Chen, Y.-F., H.-W. Wu, Y.-H. Hong, and H.-Y. Lee, "40 GHz RF biosensor based on microwave coplanar waveguide transmission line for cancer cells (HepG2) dielectric characterization," *Biosensors and Bioelectronics*, Vol. 61, 417–421, Nov. 2014.

[12] Hsiao, Y.-P., A. Mukundan, W.-C. Chen, M.-T. Wu, S.-C. Hsieh, and H.-C. Wang, "Design of a lab-on-chip for cancer cell detection through impedance and photoelectrochemical response analysis," *Biosensors*, Vol. 12, No. 6, 405, 2022.

[13] Ali, L., M. U. Mohammed, M. Khan, A. H. B. Yousuf, and M. H. Chowdhury, "High-quality optical ring resonator-based biosensor for cancer detection," *IEEE Sensors Journal*, Vol. 20, No. 4, 1867–1875, Feb. 2020.

[14] Fang, W., X. Lv, Z. Ma, J. Liu, W. Pei, and Z. Geng, "A flexible terahertz metamaterial biosensor for cancer cell growth and migration detection," *Micromachines*, Vol. 13, No. 4, 631, 2022.

[15] Pumera, M., "Graphene in biosensing," *Materials Today*, Vol. 14, No. 7-8, 308–315, 2011.

[16] Hernaez, M., "Applications of graphene-based materials in sensors," *Sensors*, Vol. 20, No. 11, 3196, 2020.

[17] Peña-Bahamonde, J., H. N. Nguyen, S. K. Fanourakis, and D. F. Rodrigues, "Recent advances in graphene-based biosensor technology with applications in life sciences," *Journal of Nanobiotechnology*, Vol. 16, 75, 2018.

[18] Hlali, A., A. Oueslati, and H. Zairi, "Numerical simulation of tunable terahertz graphene-based sensor for breast tumor detection," *IEEE Sensors Journal*, Vol. 21, No. 8, 9844–9851, 2021.

[19] Lotfi, F., N. Sang-Nourpour, and R. Kheradmand, "All-optical tunable plasmonic biosensor made of graphene and metamaterial," *Plasmonics*, Vol. 17, 799–809, 2022.

[20] Chen, S.-L., C.-Y. Chen, J. C.-H. Hsieh, Z.-Y. Yu, S.-J. Cheng, K. Y. Hsieh, J.-W. Yang, P. V. Kumar, S.-F. Lin, and G.-Y. Chen, "Graphene oxide-based biosensors for liquid biopsies in cancer diagnosis," *Nanomaterials*, Vol. 9, No. 12, 1725, 2019.

[21] Pourmadadi, M., H. S. Dinani, F. S. Tabar, K. Khassi, S. Janfaza, N. Tasnim, and M. Hoorfar, "Properties and applications of graphene and its derivatives in biosensors for cancer detection: A comprehensive review," *Biosensors*, Vol. 12, No. 5, 269, 2022.

[22] Ozkan-Ariksoysal, D., "Current perspectives in graphene oxide-based electrochemical biosensors for cancer diagnostics," *Biosensors*, Vol. 12, No. 8, 607, 2022.

[23] Rezeg, M. and H. Zairi, "A highly sensitive interdigital biosensor for cancer cells dielectric characterization using microwave frequencies," in *The Tenth International Conference on Sensor Device Technologies and Applications*, 68–71, 2019.

[24] Pourmadadi, M., H. S. Dinani, F. S. Tabar, K. Khassi, S. Janfaza, N. Tasnim, and M. Hoorfar, "Properties and applications of graphene and its derivatives in biosensors for cancer detection: A comprehensive review," *Biosensors*, Vol. 12, No. 5, 269, 2022.

[25] Yang, Y., E. Noviana, M. P. Nguyen, B. J. Geiss, D. S. Dandy, and C. S. Henry, "Paper-based microfluidic devices: Emerging themes and applications," *Analytical Chemistry*, Vol. 89, No. 1, 71–91, Jan. 2017.

[26] Syama, S. and P. V. Mohanan, "Safety and biocompatibility of graphene: A new generation nanomaterial for biomedical application," *International Journal of Biological Macromolecules*, Vol. 86, 546–555, May 2016.

[27] Kazemi, A. H. and A. Mokhtari, "Graphene-based patch antenna tunable in the three atmospheric windows," *Optik*, Vol. 142, 475–482, 2017.

[28] Krid, H. B., Z. Houaneb, and H. Zairi, "Reconfigurable rectangular ring antenna based on graphene for terahertz applications," in *2022 IEEE 21st international Ccnference on Sciences and Techniques of Automatic Control and Computer Engineering (STA)*, 695–698, 2022.

[29] Hosseininejad, S. E. and N. Komjani, "Waveguide-fed tunable terahertz antenna based on hybrid graphene-metal structure," *IEEE Transactions on Antennas and Propagation*, Vol. 64, No. 9, 3787–3793, 2016.

[30] Hu, X., G. Xu, L. Wen, H. Wang, Y. Zhao, Y. Zhang, D. R. S. Cumming, and Q. Chen, "Metamaterial absorber integrated microfluidic terahertz sensors," *Laser & Photonics Reviews*, Vol. 10, No. 6, 962–969, 2016.

[31] Nakao, M., "Sensing microscopy," *Encyclopedia of Food Microbiology*, 702–710, 2014.

[32] Sasaki, K., E. Porter, E. A. Rashed, L. Farrugia, and G. Schmid, "Measurement and image-based estimation of dielectric properties of biological tissues — Past, present, and future," *Physics in Medicine & Biology*, Vol. 67, No. 14, 2022.

[33] Nikitkina, A. I., *et al.*, "Terahertz radiation and the skin: A review," *Journal of Biomedical Optics*, Vol. 26, No. 4, 2021.

[34] Zaitsev, K. I., N. V. Chernomyrdin, K. G. Kudrin, I. V. Reshetov, and S. O. Yurchenko, "Terahertz spectroscopy of pigmentary skin nevi in vivo," *Optics and Spectroscopy*, Vol. 119, 404–410, 2015.

[35] Zaytsev, K. I., K. G. Kudrin, V. E. Karasik, I. V. Reshetov, and S. O. Yurchenko, "In vivo terahertz spectroscopy of pigmentary skin nevi: Pilot study of non-invasive early diagnosis of dysplasia," *Applied Physics Letters*, Vol. 106, No. 5, 053702, 2015.

[36] Ali, L., M. U. Mohammed, M. Khan, A. H. B. Yousuf, and M. H. Chowdhury, "High-quality optical ring resonator-based biosensor for cancer detection," *IEEE Sensors Journal*, Vol. 20, No. 4, 1867–1875, 2020.

[37] Keshavarz, A. and Z. Vafapour, "Sensing avian influenza viruses using terahertz metamaterial reflector," *IEEE Sensors Journal*, Vol. 19, No. 13, 5161–5166, 2019.

[38] Veeraselvam, A., G. N. A. Mohammed, K. Savarimuthu, and P. D. Vijayaraman, "An ultra-thin multiband refractive index-based carcinoma sensor using THz radiation," *IEEE Sensors*

Journal, Vol. 22, No. 3, 2045–2052, 2022.

[39] Azab, M. Y., M. F. O. Hameed, A. M. Nasr, and S. S. A. Obayya, "Highly sensitive metamaterial biosensor for cancer early detection," *IEEE Sensors Journal*, Vol. 21, No. 6, 7748–7755, 2021.

[40] Chen, C.-Y., Y.-H. Yang, and T.-J. Yen, "Unveiling the electromagnetic responses of fourfold symmetric metamaterials and their terahertz sensing capability," *Applied Physics Express*, Vol. 6, No. 2, 022002, 2013.

[41] Chen, X. and W. Fan, "Ultrasensitive terahertz metamaterial sensor based on spoof surface plasmon," *Scientific Reports*, Vol. 7,

No. 1, 2376–2382, 2017.

[42] Wang, B.-X., G.-Z. Wang, and T. Sang, "Simple design of novel triple-band terahertz metamaterial absorber for sensing application," *Journal of Physics D: Applied Physics*, Vol. 49, No. 16, 165307, 2016.

[43] Zhang, Y., T. Li, B. Zeng, H. Zhang, H. Lv, X. Huang, W. Zhang, and A. K. Azad, "A graphene based tunable terahertz sensor with double fano resonances," *Nanoscale*, Vol. 7, No. 29, 12 682–12 688, 2015.